Received: 24 May 2022 | Revised: 07 July 2022 | Accepted: 13 July 2022
DOI: 10.22034/ecc.2022.348728.1492
Eurasian Chemical Communications SAMI

FULL PAPER

Preparation and characterization of nickel oxide nanoparticles and its adsorption optimization for parachlorophenol

Suaad E. Hussain | Juman A. Naser*

Department of Chemistry, College of Education for Pure Science- Ibn Alhaitham, University of Baghdad, Baghdad, Iraq

This study used the precipitation method for preparing the nickel oxide nanoparticles (NiONPs). Scanning Electron Microscopy (SEM), Infrared spectroscopy (FT-IR), X-ray Diffraction (XRD), and X-ray dispersion spectroscopy (EDS) were employed for the characterization of the microstructures morphology and particle size which is produced by this method. We calculated the N2absorption-desorption isotherm, the pore structures, and specific NiONPsurface areas by Barrett-Joyner-Halenda (BJH) Langmuir and Brunauer-Emmett-Teller (BET) academic models. The sample showed flake fibers or sticks that set the diameter ranges (10-20) nm by SEM and XRD verifies. Therefore, the specific surface area was 98.794 m^2g^{-1}, pore volumes were 0.3105 cm^3g^{-1}, and the mean pore diameters were 1.85 nm. The study examined the impact of adsorption factors like adsorbent masses, initial concentrations, contact times, temperatures, ionic strengths, and pHs. The highest adsorbed para-chlorophenol could be adsorbent 0.05 g. The phenol adsorption increased by the rise of the initial concentrations and the system achieved an equilibrium state at 120 min. The adsorption capacity reduced when temperature decreased indicating the endothermic natures of system. The findings show that the adsorption ability of studied phenol increased when ionic strengths rose in a natural medium with the greatest values.

***Corresponding Author:**
Juman A. Naser
Email:juman.a.n@ihcoedu.uobaghdad.edu.iq
Tel.:+9647901235489

KEYWORDS

Adsorption; nickel oxidenanoparticles; para-chlorophenol; optimization; surface area.

Introduction

Nickel oxide (NiO) is a transition metal oxide with cubic lattice structure commonly employed in various uses such as: gas sensors [1,2], battery cathodes [3], electrochromic films [4], and catalysis [5]. As a result, numerous methods for preparing nanosized nickel oxide have been developed, including nanoparticles [6], nanoribbons [7], nanosheets [8], and nanorings [9]. The method of preparation, precursors, and precipitation agent all influence the structural and textural features of the material [10]. Because of its promising abilities in the adsorption of propionic acid [11], Cr (VI) [12], lead, cadmium [13], and malachite green dye [14], this oxide has been successfully used by many researchers in the pollutants adsorption.

Oil refining, petrochemicals, resin manufacture, coking activities, wood products, paint, paper, pulp, plastics, and pharmaceuticals have phenolic compounds in their effluents [15-17]. Discharges of these

chemicals, which are untreated could be a main concern for the health, animals, and aquatic ecosystems [15].

Phenol with hazardous health impacts could be acute and chronic. Everlasting exposures in humans can cause muscle weakness, irregular breathing, tremor, respiratory arrest, and unconsciousness at deadly concentrations. Phenol irritates the human skin, eyes, and mucous membranes. In animals, chronic phenol exposures irritates the gastrointestinal and central nervous systems, kidneys, liver, and cardiovascular tissues [18,19].

Traditional procedures such as steam distillation, oxidation, ozonation, adsorption, extraction, and biodegradation have been used for phenol removal [20,21]. Phenol adsorption on solid media such as clay, activated carbon, and transition metal oxides is one of several treatment methods that allowed for their removal from water without the use of chemicals [2,22,23].

This work prepares nickel oxide nanoparticles. A structural and textural investigation was carried out by FTIR, SEM, XRD, and N_2 gas adsorption/desorption. Thus, their usage in the adsorption of para-chlorophenol from aqueous solution. The adsorption optimizations were analyzed in different settings such as: adsorbent masses, initial concentrations, contact times, ionic strengths, pH, and temperatures. We decided to evaluate this surface in removing of phenol in aqueous mediums due to the general weak capability of phenol adsorption on many adsorbents reported in several publications.

Experimental

Chemicals

The chemical materials potassium chlorides, nickel sulfate dihydrates, ethanol, hydrochloric acids, sodium hydroxides, sodium chlorides, and para-chlorophenol have been bought from Sigma-Aldrich.

Preparation of nickel oxide nanoparticles

(6.6) g of nickel Sulfate dihydrate ($Ni(SO_4)_2.6H_2O$) was dissolved in (600) mL of distilled water. The solution was heated under constant stirring at 70°C for 1 hour. (200) mL, drop by drop (50) mL/min of Sodium solution (NaOH) was added to this solution. The resulting solid was filtered and washed with distilled water several times till the filtrated solution reached pH=7, and then it was dried at 100°Cin a vacuum oven. The dried product was calcinatedat 500°C for 3 hours.

Characterization of nickel oxide nanoparticles

FTIR: (Shimadzu, IR Affinity 1800) device was used to perform the FTIR in the range of (400 -4000) cm^{-1}.

XRD: (Shimadzu, XRD-6000) diffractometer was applied for X-rays with a monochromator to the diffracted beams by using the CuKa radiations f (k = 1.5406 A) for obtaining X-ray diffraction diagrams.

SEM: (TESCAN, IRAffinity1800) device was utilized to carry out scanning electron microscope (SEM) images of EDX.

BET and BJH analysis: The adsorption/desorption of N_2 at 196°C was performed to determine the textural property of the prepared NiONPs made by a (MINI II, BELSORP). The BET and methods were made to calculate the textural parameters.

Adsorption experiments

We performed the adsorption practical parts at constant temperatures of 25°C with stirring at (200) rpm by using a shaking water bath (Model SWB-25, HYSC) for an adsorption period. Para-chlorophenol solution (100) mg/L in (10) mL connects to a mass (0.05) g and NiONPs. The pH of the adsorption solution was modified to meet the experience needs of NaOH or HCl. The adsorption mixtures were separated by centrifuge (ModelHettich, EBA-20) at (80) rpm for (2) min and analyzed by UV/visible spectrophotometer

(ModelShimadzu, 8400S). A residual concentrations were determined based on a calibration curve at λ = 225 nm. The adsorbed value was calculated by the following equation:

$$q_e = \frac{(C_o - C_e)V}{w} (1)$$

In which, $q_e$is the adsorption capability (mg/g), C_o is the initial phenol concentrations (mg/L), m is the mass of the adsorbent (g), and V is the volume (L) of solutions.

Results and discussion

Fourier transform infrared (FT-IR)

In spectra, the produced NiONPs had peaks at 833 cm^{-1}, 740 cm^{-1}, and 686 cm^{-1}, as displayed in Figure 1. A strip to 1543 cm^{-1} and 1523 cm^{-1} was also presented to the CO_2 vibrations adsorbed form resulting from the atmospheric air. We can see a peak at 1685 cm^{-1} and 1639 cm^{-1}, as well as 3865 cm^{-1} and 3738 cm^{-1}, on the same spectrum. These peaks were corresponded to the vibration of the water's hydroxyl [9].

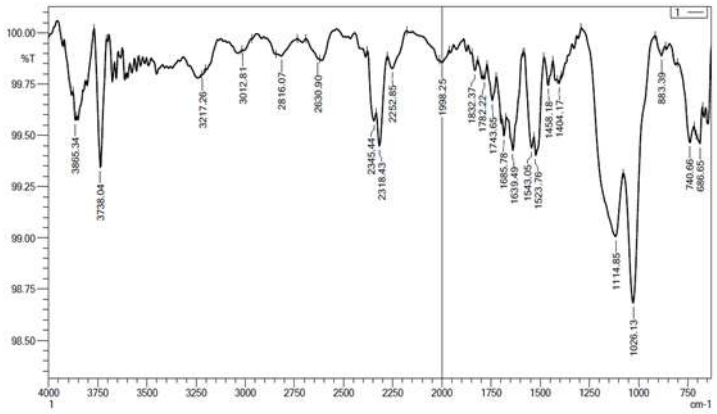

FIGURE 1 FT-IR spectra of the prepared NiONPs

Scanning electron microscope (SEM)

Microscopic photographs were acquired by using a scanning electron microscope, which helped researchers better comprehend the form and size of particles. We can observe the pure surface of NiONPs consisting of irregularly shaped grains fused together, as depicted in Figure 2. The microstructure photographs indicates that the surface of the prepared nanoparticles owned flake fibers or sticks shape with diameter range (10-20) nm. This reflects the fact that they have a huge specific surface area [24].

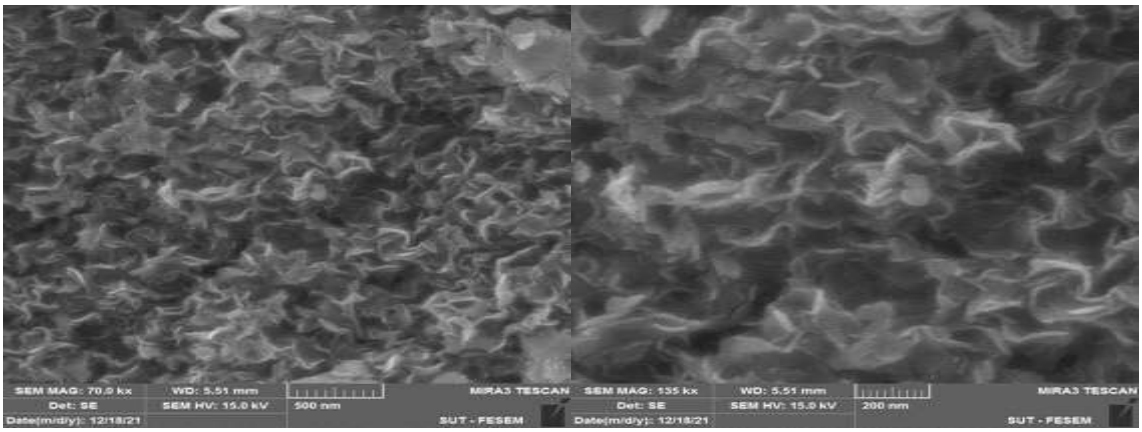

FIGURE 2 SEM photographs of the prepared NiONPs

X-ray dispersion spectroscopy (EDS)

The X-ray dispersive spectroscopy proved the availability of the NiO elements and the reduction of nickel ion to zero valences, as illustrated in Figure 3. The atomic percentage of the elemental composition of the prepared nanoparticles was 77.2% for Ni and 22.8% for O.

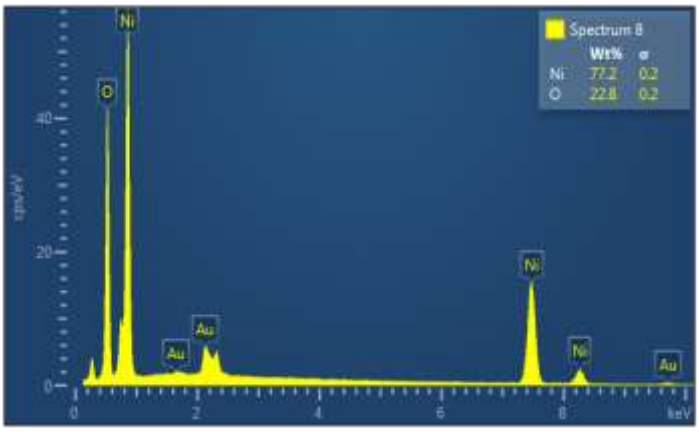

FIGURE 3 EDS spectra of the prepared NiONPs

X-ray spectroscopy (XRD)

The produced NiONPs crystalline structures were examined by the X-ray diffraction spectroscopy techniques, as demonstrated in Figure 4. The produced nanoparticles' diffraction peaks at 2θ were 31.7603°, 43.4133°, 63.1400°, and75.6349° that are possibly related to the crystalline plans 111, 200, 220, and 311, respectively. All the reflections are indexed in phase flake shapes confirming the JCPDS. The mean particle crystallite sizes reached 15 nm, according to DebyScherrer's equation [25].

$$L = \frac{0.94\,\lambda}{\beta \cos \theta} \qquad (2)$$

Where L is the size of particles (nm), λ indicates the x-ray wavelengths (nm), β stands for the full width at half optimal beams (FWHM), and finally ɵ is the Bragg angle.

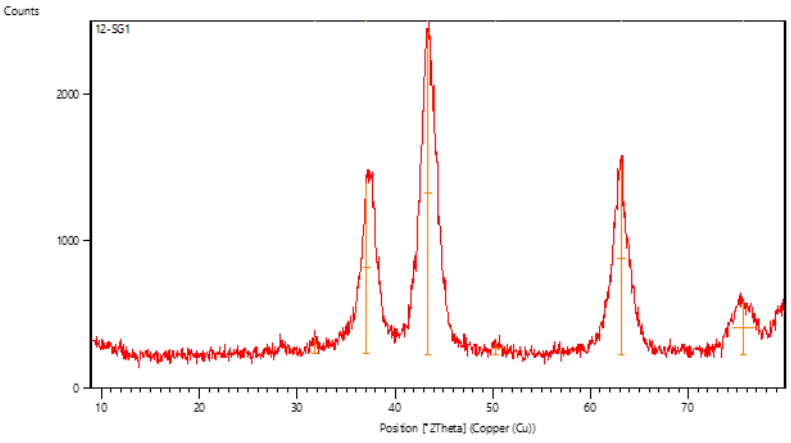

FIGURE 4 XRD spectrum of the prepared NiONPs

Surface area characteristics

The adsorbed's surface and porous surfaces are essential factors that determine adsorption. Their sizes in generated NiONPs were shown by the nitrogen gas adsorption-desorption technique. The Langmuir isotherm, Brunner-Emmett-Teller (BET), and

Barrett-Joyner-Holland (BJH) academic models were employed.

Langmuir isotherm of N_2 gas molecules adsorption-desorption on NiONPs surface is depicted in Figure 5. It is worth noting that when the pressure applied at all sites rises, it does the adsorption of gas molecules. As a result, the adsorption isotherm is labeled as type II, indicating multi-layer adsorption. As the applied pressure is lowered, the desorbed gas volume decreases at all of the pressure sites tested.

As demonstrated in Figure 6, the Brunner-Emmett-Teller (BET) diagram of nitrogen adsorption on the surface of the prepared NiONPs revealed that the number of nitrogen gas molecules increased as the applied pressure increased and they reached the maximum value at 0.45 at 0.029 P/P°. This indicates that NiONPs will adsorb nitrogen gas molecules at any of the tested pressures.

The nitrogen gas molecule adsorption on the outer layer of the prepared NiONPs is indicated in Figure 7B of the JH diagram. The mean pore size is 1.85 nm, with a pore volume of 0.3105 cm^3g^{-1} and nanoparticle surface areas of 98.794 m^2g^{-1}. Overall, the BET and BJH diagrams of the analyzed NiONPs outer layer do not account for the BJH model discrepancies to the micro pores [26].

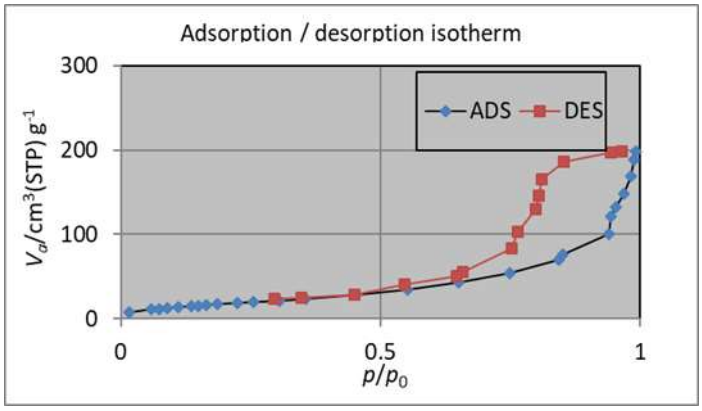

FIGURE 5 Adsorption- desorption of Langmuir isotherm of the prepared NiONPs

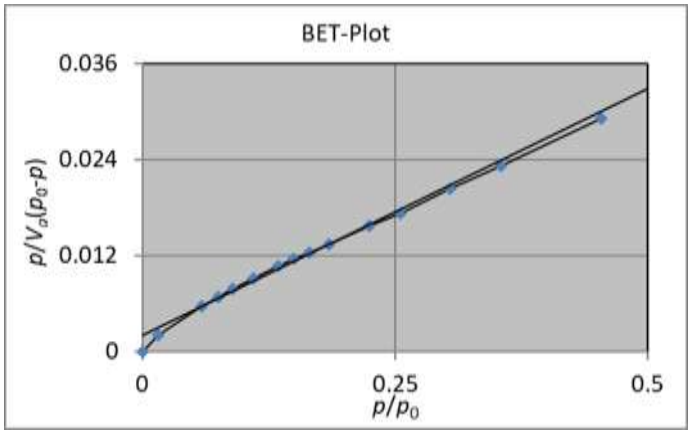

FIGURE 6 BET plot of adsorption of the prepared NiONPs

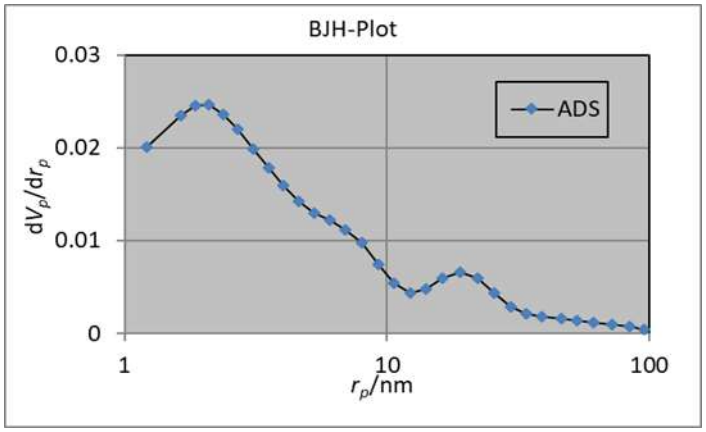

FIGURE 7 BJH plot of adsorption of the prepared NiONPs

Adsorbent mass effect

The effect of adsorbent mass of the prepared NiONPs on the adsorption of para-chlorophenol with a primary concentration of 20 mg/L at 25℃ was investigated, as displayed in in Figure 8. The adsorbed amount of phenol increases as the mass of the adsorbent outer layer increases when the outer layer increases, and thus the adsorption sites increase [27]. The adsorbent mass became ineffective after the greatest absorbed amount of para-chlorophenol when reached 0.05 g of adsorbent, indicating that saturation had been attained.

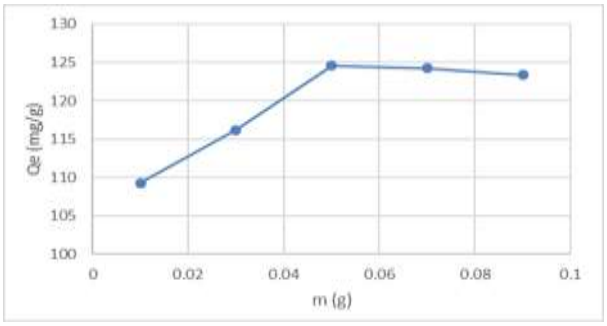

FIGURE 8 Adsorbent mass effect of para-chlorophenol adsorption on NiONPs

Initial concentration effect

The first impact concentration of para-chlorophenol adsorption on NiONPs at concentrations of (5, 10, 15, 20, and 25) mg/L, the adsorbent mass of 0.05 g, and temperature of 25℃ was investigated, as depicted in Figure 9. As the para-chlorophenol concentration is increased, the adsorbed amount decreases indicating that adsorption capacity is lowering. Thus, the steric obstruction is due to the crowding of para-chlorophenol molecules on the adsorbent outer layers.

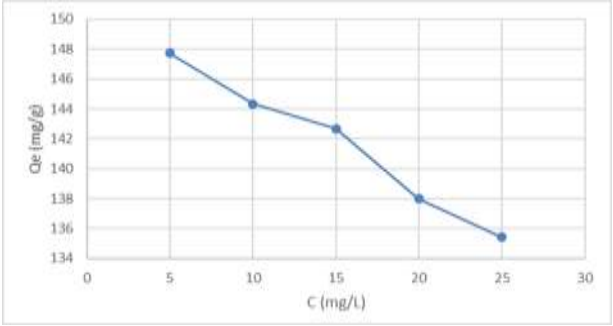

FIGURE 9 Initial concentration effect of para-chlorophenol adsorption on NiONPs

Contact time effect

At the initial concentration of 20 mg/L, the adsorbent masses were 0.05 g, and temperature was 25°C, the contact time effect of para-chlorophenol on NiONPs was examined, as indicated in Figure 10. The adsorbed quantity grows with time till stabilizing for 120 min, indicating equilibrium of the adsorption as the adsorbed molecules of para-chlorophenol saturate each site on the adsorbent surfaces [28].

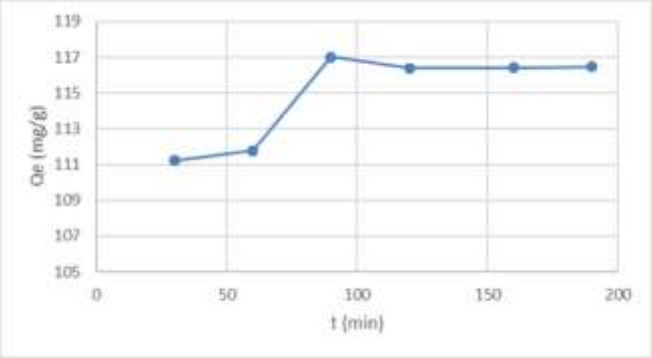

FIGURE 10 Contact time effect of para-chlorophenol adsorption on NiONPs

Ionic strength effect

The effect of ionic strengths of para-chlorophenol adsorption on NiONPs was investigated by using (0.1, 0.2, 0.3, and 0.4) M of NaCl and KCl as concentrations at a first concentration of 20 mg/L, adsorbent masses of 0.003 g, and temperatures of 298 K, as illustrated in Figure 11. Because the salt accumulates the para-chlorophenol molecules in the solution, the adsorption capacities was improved with the rise in the ionic strength, based on the findings. As a result, para-chlorophenol hydrophobicity increases and solubility in water decreases, allowing for increased adsorption capacity [29].

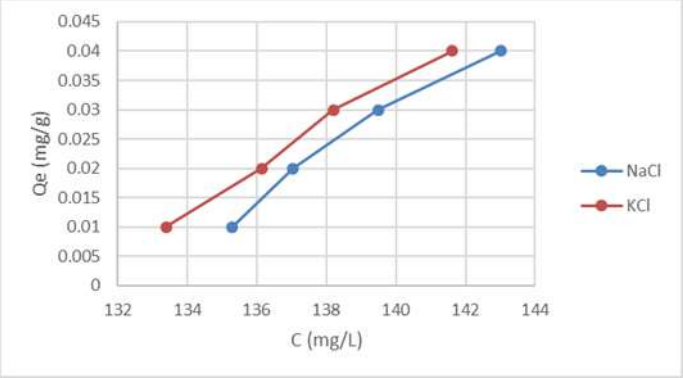

FIGURE 11 Ionic strength effect of para-chlorophenol adsorption on NiONPs

pH Effect

Figure 12 reveals the pH impact on para-chlorophenol adsorption on NiONPs at a primary concentration of 20 mg/L, an adsorbent mass of 0.05 g, and a temperature of 298 K. The data revealed that the adsorption capacity is highest in the acidic medium and decreases as the pH of the solution rises. Thus, in an alkaline media, electrostatic repulsion accumulates, increasing the negative charge of the surface and inhibiting anionic molecule attraction to the adsorbed surface [30].

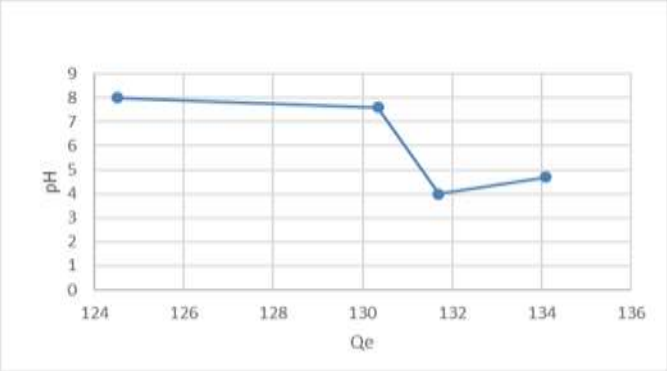

FIGURE 12 pH effect of para-chlorophenol adsorption on NiONPs

Conclusion

The optimal precipitation method was used for successful preparation of the nickel nanoparticles, NiONPs. This method uses (FT-IR), SEM), X- (EDS), and (XRD). It produced nanoparticles with similar sizes and higher purities. The nanoparticles showed flake fibers or sticks shape with a diameter range of (10-20) nm, based on the mean equivalent particle size which SEM indicates and XRD and BET data is verified. The BET adsorption equation shows that the sample's specific outer cover is 98.794 m^2g^{-1}. The cumulative pore volumes are 0.3105 cm^3g^{-1}, while the mean pore diameter reaches 1.85 nm, according to the BJH model.

The study examined the influence some aspects like adsorbent masses, the initial concentrations, contact times, temperatures, ionic strengths, and pH that were investigated. Nickel nanoparticles NiONPs have is efficient in para-chlorophenol adsorption from the aqueous solution. The largest adsorption amount reached 0.05 g of the adsorbent with a positive correlation with the primary concentrations. The examined system reaches an equilibrium at 120 min. Thus, the negative correlation between the adsorbed phenol capacity and temperature shows the adsorption system endothermic nature. The findings indicate there is a positive correlation between the adsorption capacity increases and ionic strengths as a natural media with the highest value.

Acknowledgements

The authors are grateful to Department of Chemistry, College of Education for Pure Science- Ibn Alhaitham, University of Baghdad for an achieving the practical part of this work.

Orcid:
Suaad E. Hussain:
https://www.orcid.org/0000-0003-1408-0278
Juman A. Naser:
https://www.orcid.org/0000-0003-2319-5384

References

[1] K.P. Gautam, D. Acharya, I. Bhatta, V. Subedi, M. Das, S. Neupane, J. Kunwar, K. Chhetri, A.P. Yadav, *Inorganics*, **2022**, *10*, 86. [Crossref], [Google Scholar], [Publisher]
[2] A. Mandal, S.K. Das, *J. Environ. Chem. Eng.*, **2019**, *7*, 103259. [Crossref], [Google Scholar], [Publisher]
[3] X. Li, C. Wen, M. Yuan, Z. Sun, Y. Wei, L. Ma, H. Li, G. Sun, *J. Alloys Compd.*, **2020**, *824*, 153803. [Crossref], [Google Scholar], [Publisher]
[4] T.P. Mokoena, H.C. Swart, D.E. Motaung, *J. Alloys Compd.*, **2019**, *805*, 267-294. [Crossref], [Google Scholar], [Publisher]
[5] T. Lim, K. Seo, S.M. Jeong, S. Ju, *AIP Adv.*, **2020**, *10*, 085319. [Crossref], [Google Scholar], [Publisher]
[6] A.J. Haider, R. Al-Anbari, H.M. Sami, M.J. Haider, *Energy Procedia,* **2019**, *157*, 1328-1342.[Crossref], [Google Scholar], [Publisher]
[7] K. Matsui, B.K. Pradhan, T. Kyotani, A. Tomita, *J. Phys. Chem. B,* **2001**, *105*,5682-5688.[Crossref], [Google Scholar], [Publisher]

[8] A.K. Patra, S. Sarkar, D. Kim, *Mater. Res. Bull.,* **2021**, *139*, 111251. [Crossref], [Google Scholar], [Publisher]
[9] M.E. Begum, M.N.A. Chowdhury, M.B. Islam, *Results in Materials*, **2022**, *14*, 100265. [Crossref], [Google Scholar], [Publisher]
[10] Y. Dehmani, S. Abouarnadasse, *Arab. J. Chem.,* **2020**, *13*, 5312-5325. [Crossref], [Google Scholar], [Publisher]
[11] A. El-Qanni, N.N. Nassar, G. Vitale, *Chem. Eng. J.,* **2017**, *327*, 666-677. [Crossref], [Google Scholar], [Publisher]
[12] M.A. Behnajady, S. Bimeghdar, *Chem. Eng. J.,* **2014**, *239*, 105-113.[Crossref], [Google Scholar], [Publisher]
[13] P.R. Sardar, *Indian J. Sci. Technol.,* **2021**, *14*, 2327-2336.[Crossref], [Google Scholar], [Publisher]
[14] H.H. El-Feky, R.N. Nassar, A.S. Amin, M.Y. Nassar, *Asian J. Chem. Sci.*, **2021**, *10*, 41-51.[Crossref], [Google Scholar], [Publisher]
[15] K. Altuntas, E. Debik, D. Kozal, I.I. Yoruk, *Period.Eng. Natur. Sci.,* **2017**, *5*. [Crossref], [Google Scholar], [Publisher]
[16] A.A. Alkaabi, A.A. Obaid, M.H. Abdulsada, *Period. Eng. Nat. Sci.,* **2021**, *10*, 212-227.[Crossref], [Google Scholar], [Publisher]
[17] H.M.A. Tameemi, A.A. Obaid, H.H. Alaydamee, A.H. Abbar, *Period. Eng. Nat. Sci.,* **2021**, *9*, 998-1015.[Crossref], [Google Scholar], [Publisher]
[18] D. Doughmi, L. Bennis, A. Berrada, A. Derkaoui, A. Shimi, M. Khatouf, *Case Rep. Crit. Care*, **2019**, *2019*, 6756352.[Crossref], [Google Scholar], [Publisher]
[19] A.M. Hammam, M.S. Zaki, R.A. Yousef, O. Fawzi, *Adv. Environ. Biol.*, **2015**, *9*, 38-49. [Crossref], [Google Scholar], [Publisher]
[20] W.H. Saputera, A.S. Putrie, A.A. Esmailpour, D. Sasongko, V. Suendo, R.R. Mukti, *Catalysts,* **2021**, *11*, 998.[Crossref], [Google Scholar], [Publisher]
[21] J.A. Naser, Z.W. Ahmed, E.H. Ali, *Mater.Today Proc.,* **2021**,*42*, 2590-2595. [Crossref], [Google Scholar], [Publisher]
[22] K.S.A. Al-Saade, H.N. AL-Ani, *Baghdad Science Journal,* **2016**, *13*, 325-361. [Google Scholar], [Publisher]
[23] Z.A.H. Al-Dulaimy, *Ibn AL-Haitham Journal For Pure and Applied Sciences,* **2017**, *30*, 118-130. [Google Scholar], [Publisher]
[24] J.P. Kumar, S.D. Giri, A. Sarkar, *Int. J. Hydrog. Energy,* **2018**, *43*, 15639-15649. [Crossref], [Google Scholar], [Publisher]
[25] S.A. Jadoo, J.A. Naser, *IOP Conf. Ser.: Mater. Sci. Eng.*, **2020**, *928*, 052024. [Crossref], [Google Scholar], [Publisher]
[26] R.S. Sahib, J.A. Naser, *Ann. Romanian Soc. Cell Biol.*, **2021**, *25*, 2962-2969. [Google Scholar], [Publisher]
[27] A.M. Aljeboree, A.N. Alshirifi, A.F. Alkaim, *Arab. J. Chem.,* **2017**, *10*, S3381-S3393.[Crossref], [Google Scholar], [Publisher]
[28] S.A. Jadoo, J.A. Naser, *J. Glob. Pharma Technol.,* **2019**, *11*, 401-411. [Google Scholar], [Publisher]
[29] S. Wang, N. Qiao, J. Yu, X. Huang, M. Hu, H. Ma, *Desalination Water Treat.,* **2016**, *57*, 4174-4182. [Crossref], [Google Scholar], [Publisher]
[30] J.C. Lazo-Cannata, A. Nieto-Márquez, A. Jacoby, A.L. Paredes-Doig, A. Romero, M.R. Sun-Kou, J.L. Valverde, *Sep.Purif. Technol.,* **2011**, *80*, 217-224. [Crossref], [Google Scholar], [Publisher]

How to cite this article: Suaad E. Hussain, Juman A. Naser*. Preparation and characterization of nickel oxide nanoparticles and its adsorption optimization for parachlorophenol. *Eurasian Chemical Communications*, 2022, 4(12), 1209-1217. **Link:** http://www.echemcom.com/article_153480.html